Rakenteiden Mekaniikka (Journal of Structural Mechanics)
Vol. 58, No. 2, 2025, pp. 59–70
http://rakenteidenmekaniikka.journal.fi
https://doi.org/10.23998/rm.152469

VERTAISARVIOITU
KOLLEGIALT GRANSKAD
PEER-REVIEWED
www.tsv.fi/tunnus

Simulation of hydrogen-induced failure in high strength steel

Stefan Lampenscherf [1] and Gia Khanh Pham

Summary We present a coupled chemo-mechanical and fracture mechanics-based model capable of predicting the onset of hydrogen-induced macroscopic crack growth as a function of material, loading and environmental variables. The model is implemented using the commercial multi-physics simulation package COMSOL and solved as a coupled deformation–diffusion problem to define a fracture criterion as a function of residual and externally applied loads and hydrogen concentration. The local hydrogen-induced material damage is approximated by a parametric dependency of local fracture resistance on hydrogen concentration. As an example, we demonstrate the ductile-brittle transition of the failure pattern of a double-notch specimen under tension w/o and w/ hydrogen loading.

Keywords: hydrogen embrittlement, hydrogen transport model, chemo-mechanical and *fracture mechanics-based failure model, hydrostatic process zone, COMSOL Multiphysics, ductile-brittle transition,* FEM-simulation

Received: 29 November 2024. Accepted: 2 June 2025. Published online: 23 June 2025.

Introduction

When exposed to hydrogen, many metallic materials experience a significant loss of ductility, toughness and fatigue crack growth resistance [1, 2, 3]. This phenomenon, known as hydrogen embrittlement (HE), is a major challenge for the development of advanced high strength steel applications (e.g. in the construction, transport and energy sectors) due to the ubiquity of hydrogen and the higher susceptibility of modern high-strength alloys [4, 5].

The main reason for HE vulnerability is the complex microstructure of high strength steels. Structural features like dislocations, grain/phase boundaries and precipitates in combination with non-homogenous stress distributions and plastic deformation lead to

[1]Corresponding author: lightsharp30@outlook.de

local hydrogen accumulation and promote material failure by means of mechanisms that are still being debated [6, 7, 8, 9] .

Macroscopic prediction of hydrogen-induced failure and its kinetics is key for adapted design and safe usage of high strength steel components. In this paper, we present a coupled chemo-mechanical and fracture mechanics-based model that covers the complexity of hydrogen transport and damage and is capable of predicting macroscopic crack growth as a function of material, loading and environmental variables. The model is implemented using the commercial multi-physics simulation package COMSOL and solved as a coupled deformation–diffusion problem to define a fracture criterion as a function of residual and externally applied loads and hydrogen concentration. The local hydrogen-induced material damage is approximated by a parametric dependency of local fracture toughness on hydrogen concentration in the hydrostatic process zone near the crack tip (strain concentrator). In order to proof the capability of the simulation method, we demonstrate a ductile-brittle transition in the failure pattern of a double edge notched specimen under tension with and without hydrogen charging.

Theoretical background: hydrogen uptake and transport

Hydrogen ingress into steel can occur during manufacturing operations, such as casting, welding, machining or electroplating, and through exposure to hydrogenous environments such as water vapor, aqueous electrolytes or hydrogen-containing gas. Following ingress, atomic hydrogen resides at either interstitial lattice sites or microstructural trapping sites (e.g. dislocations, grain boundaries, voids, carbides and interfaces).

The transport of hydrogen in steel is primarily enabled by diffusion of hydrogen on interstitial lattice sites. Applying the general Nernst–Planck equation, the hydrogen flux density $\boldsymbol{j}$ is driven by the gradient of the chemical potential μ of atomic hydrogen on interstitial lattice sites [10]

$$\boldsymbol{j} = -\frac{D\, c_l}{R\, T}\boldsymbol{\nabla}\mu \tag{1}$$

with D as hydrogen diffusivity, c_l as lattice hydrogen concentration (hydrogen on interstitial lattice sites), T as absolute temperature and R as universal gas constant. In the practical case of low hydrogen occupancy of interstitial sites $c_l / N_l << 1$ (N_l … number of interstitial lattice sites per unit volume) the chemical potential μ is given by [10]

$$\mu = \mu_0 + \mathrm{R\,T\,ln}\left(\frac{c_l}{N_l}\right) - \sigma_h \mathrm{V_H} \quad \text{with} \quad \sigma_h = \frac{1}{3}\, tr\left(\sigma_{ij}\right). \tag{2}$$

σ_H denotes the hydrostatic stress and V_H the partial molar volume of hydrogen (see Tab.1). Combining equations (1) and (2) we obtain the hydrogen flux density $\boldsymbol{j}$

$$\boldsymbol{j} = -D\,\boldsymbol{\nabla} c_l + \frac{D\, c_l V_H}{R\, T}\boldsymbol{\nabla}\sigma_h. \tag{3}$$

According to (3) external or residual stresses affect hydrogen diffusion by generating hydrostatic stress gradients. Tensile hydrostatic stresses extend the volume of the interstitial lattice sites, whereas compressive stresses lead to the lattice sites volume

reduction. As a result, dissolved hydrogen atoms tend to move to areas of tensile hydrostatic stress (e.g. notches, crack tips) where damage takes place.

As mentioned above, hydrogen does not only reside on interstitial lattice sites, but can also be trapped by microstructural features such as point defects, dislocations, precipitates, grain/phase boundaries, etc. Therefore, the total concentration of hydrogen is the sum of lattice hydrogen concentration c_l and trapped hydrogen concentration $c_{t,i}$ [3] where i is the index of the trap type

$$c_{tot} = c_l + \sum_i c_{t,i} \ . \tag{4}$$

With the presence of traps, the diffusion of hydrogen is modified by trapping and detrapping of hydrogen atoms [11]. Mass conservation dictates that the rate of change of total hydrogen concentration equals the net flux of diffusing hydrogen atoms

$$\frac{\partial c_{tot}}{\partial t} = -\boldsymbol{\nabla} \cdot \boldsymbol{j} \ . \tag{5}$$

Following Oriani [12], the rate of trapping and detrapping is sufficiently fast for local equilibrium to exist between hydrogen atoms at lattice sites and trap sites. For the practical case of low occupation of lattice sites $\theta_l = c_l/N_l << 1$ we get functional relationships between occupation of traps $\theta_{t,i} = c_{t,i}/N_{t,i}$ and occupation of lattice sites [11]

$$\theta_{t,i} = \frac{\theta_l}{\theta_l + K_{t,i}} \qquad \text{(i … index of trapping site).} \tag{6}$$

$N_{t,i}$, $E_{t,i}$ and $K_{t,i} = \exp\left(\frac{-E_{t,i}}{RT}\right)$ are the number of trapping sites per unit volume, the hydrogen binding energy and the equilibrium constant for type i trapping site respectively. With (4) and (6) the rate of change of total hydrogen concentration becomes

$$\frac{\partial c_{tot}}{\partial t} = \left(1 + \frac{\partial \sum_i c_{t,i}}{\partial c_l}\right) \frac{\partial c_l}{\partial t} \ . \tag{7}$$

Introducing an effective diffusivity

$$D_{eff} = D \left(1 + \frac{\partial \sum_i c_{t,i}}{\partial c_l}\right)^{-1} \tag{8}$$

we can use (3), (5) and (7) to obtain a coupled chemo-mechanical diffusion equation for hydrogen transport in steel with complex microstructure

$$\frac{\partial c_l}{\partial t} = D_{eff} \nabla^2 c_l - \frac{D_{eff} V_H}{R \cdot T} \boldsymbol{\nabla} \cdot (c_l \boldsymbol{\nabla} \sigma_h) \ . \tag{9}$$

D refers to the hydrogen diffusivity in the perfect lattice (no microstructural effects) and takes the form

$$D = D_0 \, exp\left(-\frac{Q}{R \cdot T}\right). \tag{10}$$

Typical values of the preexponential factor D_0 and lattice activation energy Q for pure iron (α-Ferrite, γ-Austenite) are given in Tab.1. As an example, the effective hydrogen diffusivity D_{eff} of a ferritic steel according to trapping theory is plotted in Fig. 1 alongside with the hydrogen diffusivity of the pure iron allotropes. The diffusivity of the ferritic steel is calculated using expressions (6), (8) and (10) assuming two trap types with the parameters $N_{t,i}$ and $E_{t,i}$ *(i = 1,2)* and D_0, Q for α-Ferrite (see Tab. 1).

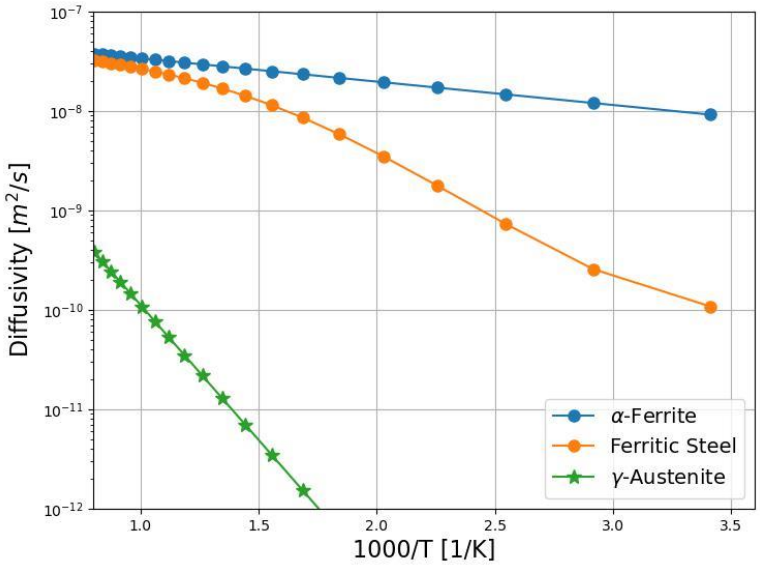

Fig. 1: Temperature dependent hydrogen diffusivity D of pure iron and D_{eff} of ferritic steel according to (6), (8) and (10) with two trap types. Parameters are given in Tab. 1.

Method for damage evolution

Hydrogen embrittlement is characterized by a loss of ductility and fracture resistance with the increase of H-concentration. A number of micro-mechanical mechanisms have been identified (e.g., microvoid coalescence, quasi-cleavage fracture), but a detailed understanding is still subject of current research [13].

In this study we use a simplified phenomenological model in order to capture the damaging effect of hydrogen accumulated in the hydrostatic tensile stress zone ahead of stress concentrators (notches, cracks). Therefore, the local hydrogen-induced material damage is approximated by a parametric dependency of local fracture resistance (critical energy release rate G_c) on lattice hydrogen concentration [14]

$$G_c(c_l) = (1 - \chi\, c_l) G_{c,0} \tag{11}$$

with χ as a hydrogen damage coefficient and $G_{c,0}$ as critical energy release rate of the undamaged material. Following [14] the reduction of Gc is primarily linked with the occupation of relevant hydrogen traps at the decohering interface. For ferritic steels we assume a trap binding energy of $E_{t,gb} = 25kJ/mol$ [15] at the decohering interface resulting in $\chi = 0.015\ m^3/mol$ at $T = 293K$.

The evolution of fracture is modeled using a phase field approximation. This means the sharp crack geometry is regularized by the nonlocal phase field in the domain material, which makes the crack path independent of the mesh elements. The driving force for damage depends on the state of deformation in the solid, which governs the evolution of the phase field. In turn, the phase field determines the degradation of the solid properties in the damaged regions. The phase-field modeling of fracture is intrinsically a multi-field coupling approach, and, therefore, can be readily extended to damage simulation in multi-physics problems. We use the AT1 phase field model [16] implemented in COMSOL and solve it in multi-field coupling with the deformation–diffusion problem to define a

fracture criterion as a function of residual and externally applied loads and hydrogen concentration. The only material input to the damage model is the critical energy release rate according to expression (11) and a regularization parameter l_{int} that controls the width of the localized phase field. It is a common consensus that l_{int} should be understood as the material's characteristic length scale linked to the material strength [17]

$$l_{int} = \frac{3EG_c}{8\,\sigma_Y^2} \quad \text{(AT1 model, plane stress).} \qquad (12)$$

With this adjustment of the regularization parameter, the phase-field models are capable of quantitative prediction of crack nucleation in a wide range of geometries and load cases [17]. For the sake of simplicity, we have substituted the material strength in (12) by the yield stress σ_Y.

Results

Transport simulation

The coupled chemo-mechanical diffusion equation (9) is implemented in the multi-physics simulation package COMSOL using the transport in solids interface and solved as a coupled deformation–diffusion problem to model both the concentration and stress driven hydrogen diffusion. We consider a single edge notched square plate of ferritic steel under static tensile load (Fig. 2). Material parameters are summarized in Tab. 1.

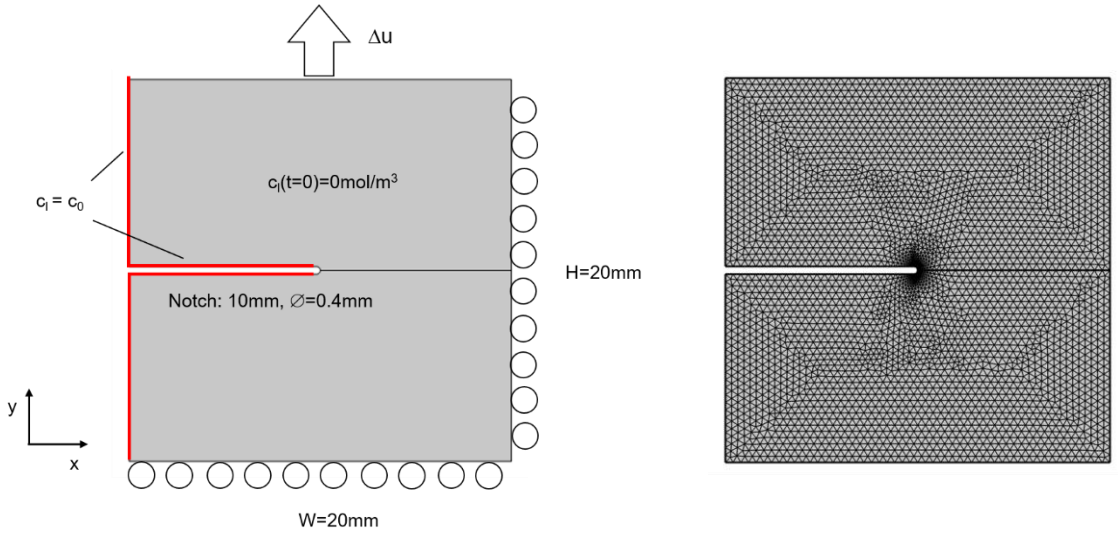

a) b)

Fig. 2: Single edge notched ferritic steel plate for chemo-mechanical transport simulation a) geometry and boundary conditions, b) simulation mesh (min. element size =0.05mm)

The ferritic steel plate is constrained on the bottom and right edges with a roller boundary condition. A prescribed displacement Δu is applied at $t = 0s$ on the top boundary to produce a mechanical load and study its effect on hydrogen diffusion. Initially, the solid is assumed hydrogen free ($c_l = 0$). The environment and surface reactions during hydrogen uptake are not modeled explicitly, instead we use the highly simplifying

assumption of constant hydrogen concentration at the charging surface, i.e. $c_l = c_0$ at the left boundary and in the notch (except notch tip). The other boundaries including front and backside are assumed to be impermeable for hydrogen.

Fig. 3a shows the spatial distribution of hydrostatic stress and the deformed geometry. The contour lines (σ_h = *75, 100, 125, 200, 400MPa*) highlight the zone of increased hydrostatic tensile stress in the vicinity of the notch. The line plot Fig. 3b clearly shows the steep increase of σ_h when approaching the notch. At the notch tip (x = *10mm*) the hydrostatic stress is limited by the yield stress: $\sigma_{h,tip} = 1/3 \cdot \sigma_Y = 200\ MPa$ ($\sigma_Y = 600MPa$, von Mises). The higher peak value of σ_h ahead of the notch is a result of the multiaxial stress state ahead of the notch.

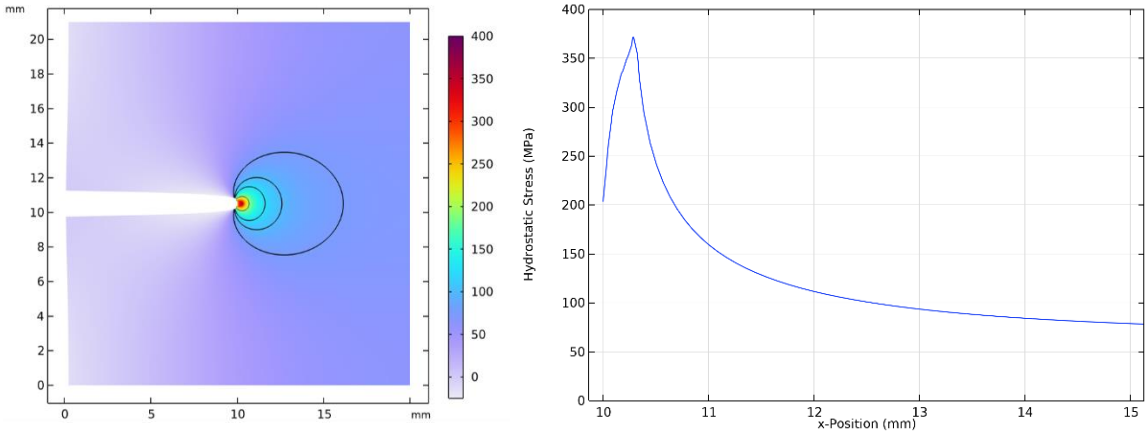

a) b)

Fig. 3: a) Color map and contour plot of hydrostatic stress σ_h [MPa] in deformed geometry (50x), b) line plot of σ_h in front of notch for Δu=*0.02mm* (*0.1% strain*)

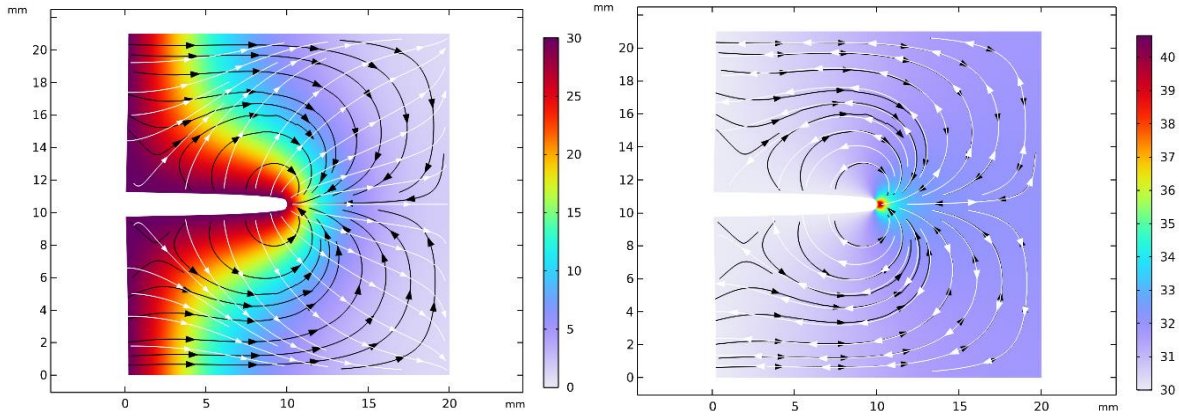

a) b)

Fig. 4: Color-map of c_l *[mol/m^3]*, concentration-driven (white) and stress-driven hydrogen flux (black) at a) 24h and b) steady state in deformed configuration (50x) for $c_0 = 30mol/m^3$

After mechanical loading hydrogen transport is simulated at $T = 293K$ assuming an effective hydrogen diffusivity $D_{eff} = 10^{-10} m^2/s$ (ferritic steel) and a hydrogen concentration $c_0 = 30mol/m^3$ at the charging surface. Figs.4a and 4b show the distribution

of lattice hydrogen concentration, concentration-driven flux (white) and stress-driven hydrogen flux (black) after 24h and in steady state condition respectively.

The stress-induced hydrogen flux (black) and steady state lattice hydrogen distribution in Fig. 4b indicate the enhanced hydrogen adsorption driven by the increased hydrostatic stress in the vicinity of the notch tip. The time-dependent development and steady state distribution of lattice hydrogen concentration in the vicinity of the notch can be assessed from the line plots Fig. 5.

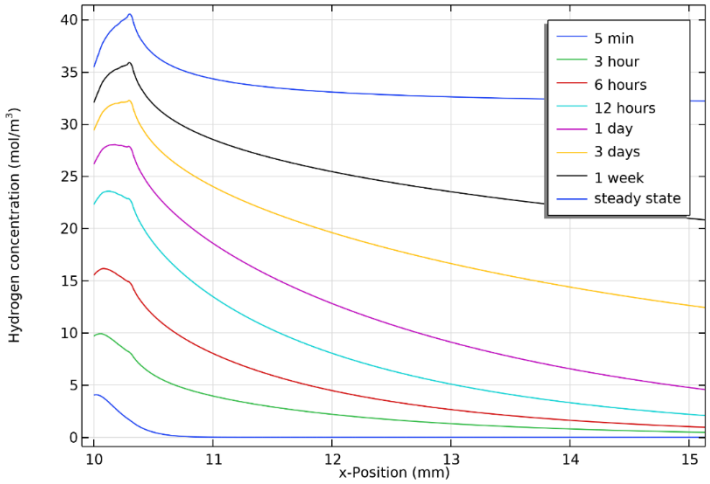

Fig. 5: Line plots of lattice hydrogen concentration c_l in front of notch

In steady state the local hydrogen concentration (Fig. 5) is linked to the local hydrostatic stress state (Fig. 3b), since thermodynamic equilibrium requires a constant chemical potential μ throughout the part. Using expression (2) we can set equal the chemical potential of hydrogen at the free edges $\mu(c = c_0, \sigma_h = 0)$ with chemical potential of hydrogen at the notch tip $\mu(c = c_{tip}, \sigma_h = \sigma_{h,tip})$. As a result, we get the following relation

$$\frac{c_{tip}}{c_0} = \exp\left(\frac{\sigma_{h,tip}\, V_H}{R\, T}\right) \tag{13}$$

also known as modified Sieverts law. With a local hydrostatic stress $\sigma_{h,tip} = 200MPa$ at the notch tip (see Fig. 3b) and $c_0 = 30mol/m^3$ expression (13) predicts a steady state lattice hydrogen concentration $c_{tip} = 35.4\ mol/m^3$ at the notch tip. This is in good agreement with the line plot of steady state lattice hydrogen concentration (Fig. 5) at the notch tip ($x = 10mm$).

Damage simulation

In the following we demonstrate the capability of the model and simulation method to capture the effect of hydrogen embrittlement on the failure pattern. Therefore, we consider a tensile test of a double edge notched ferritic steel plate (Fig. 6).

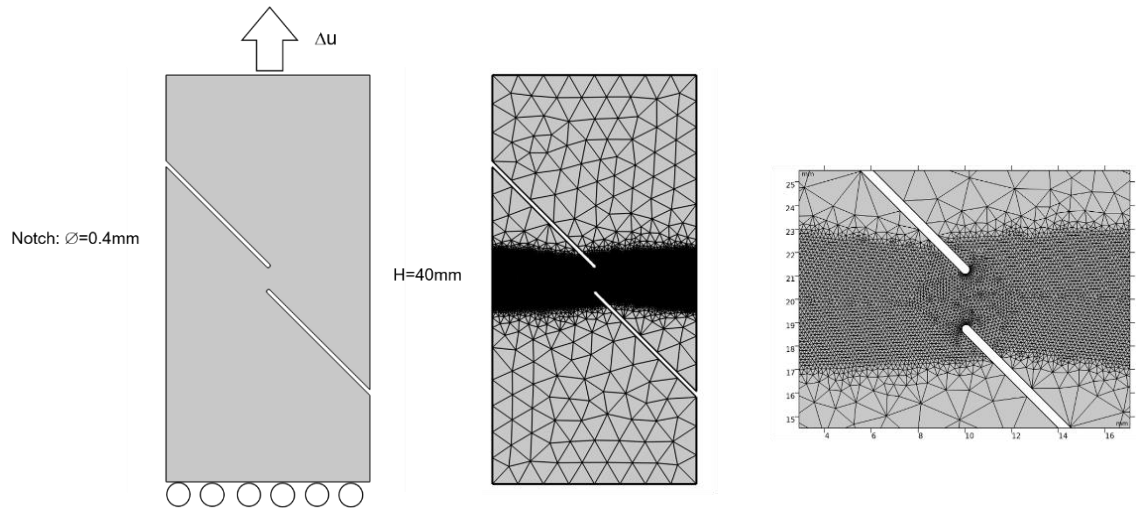

a) b)

Fig. 6: Double edge notched ferritic steel plate for damage simulation: a) geometry and boundary conditions, b) simulation mesh (min. element size 0.04mm)

To properly resolve the phase field and to achieve a stable material behavior, a high mesh density is required in the vicinity of the propagating crack. The regularization length l_{int} can be considered as being the upper limit of the appropriate mesh size. Using expression (12) with the material parameters given in Tab.1 the regularization length is l_{int} = 0.4mm. We use a finer mesh size ~1/10 l_{int} to better resolve the phase field and yield a more stable material behavior.

The damage simulation during tensile testing is performed for two samples: i) without hydrogen charging and ii) with hydrogen pre-charging of $c_l = 30mol/m^3$. The mechanical load (tension) is applied in a quasi-stationary manner maintaining steady state conditions in the latter case. Material parameters of the ferritic steel samples are summarized in Tab.1

Fig. 7 shows the hydrostatic tensile stress distribution for a tensile load of $\Delta u = 0.02mm$ (0.05 % overall tensile strain). At this point local plastic deformation near the notch tip has started. For the pre-charged sample (case ii) we can estimate the local hydrogen concentration at the notch tip using (13): $c_l = 35mol/m^3$. According to parametric damage law (11) this will cause a 50% reduction of the ferritic steel fracture resistance G_c near the notch tip of the pre-charged sample ii.

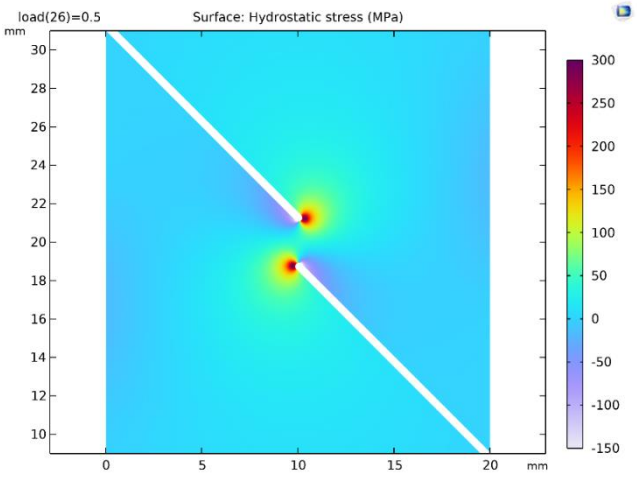

Fig. 7: hydrostatic stress distribution at $\Delta u = 0.02mm$ (0.05% overall tensile strain).

Upon further loading $\Delta u = 0.04mm$ (0.1% overall tensile strain) sample (i) develops significant plastic deformation between the notches (shear band) characteristic for a ductile failure (Fig. 8a). In contrast, further loading of sample (ii) initiates cracks from the notch tips. The cracks drive the zone of increased hydrostatic stress/hydrogen concentration in front of the crack tip and thus also the zone of hydrogen damage/reduced fracture resistance causing a brittle failure scenario (Fig. 8b).

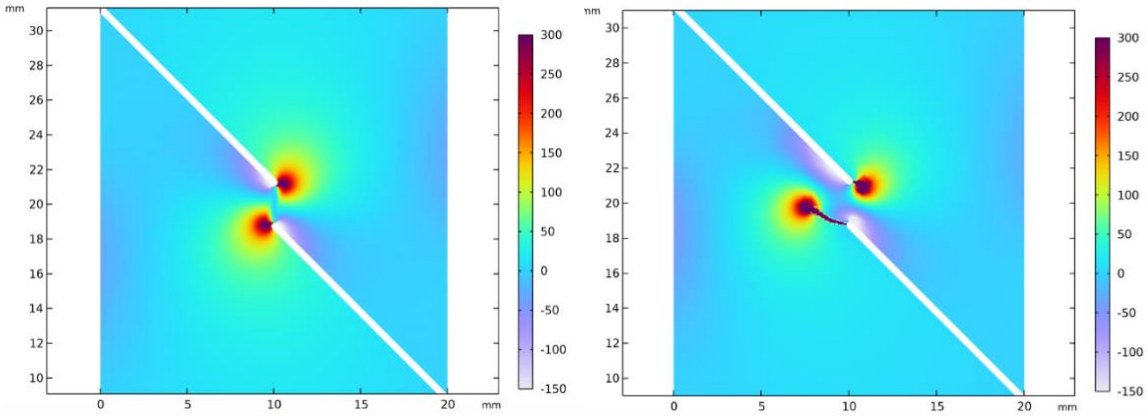

a) b)

Fig. 8: Hydrostatic stress distribution at $\Delta u = 0.04mm$: a) sample (i) w/o hydrogen charge (ductile failure), b) sample (ii) with hydrogen charge (onset of brittle failure)

Table 1. Model Parameters

Parameter	Value
Universal gas constant (R)	8.3141 J/(mol·K)
Partial molar H volume (V_H) in ferrite	$2.0\ 10^{-6}$ m^3/mol [18]
Lattice site density (N_l) in ferrite	10^6 mol/m^3
α-Ferrite: diffusion parameter (D_0, Q)	$5.8\ 10^{-8}$ m^2/s, 4.5 kJ/mol [19]
γ-Austenite: diffusion parameter (D_0, Q)	$9.9\ 10^{-7}$ m^2/s, 52 kJ/mol [20]
Temperature (T)	293.15 K
Ferritic steel parameter	
Trap binding energy ($E_{t,1}$, $E_{t,2}$)	10 kJ/mol, 25 kJ/mol
Number of trap sites ($N_{t,1}$, $N_{t,2}$)	$2\ 10^4$ mol/m^3, 10^4 mol/m^3
Youngs modulus (E)	200 GPa
Poisson ratio (ν)	0.29
Yield stress (σ_Y)	600 MPa
Critical Energy Release Rate ($G_{c,0}$)	2000 J/m^2

Conclusions

A physically motivated, macroscopic hydrogen transport and damage model has been presented and solved as a coupled deformation–diffusion problem using he multi-physics simulation package COMSOL. The simultaneous calculation of the stress field and the time-dependent local hydrogen concentration was realized. The local hydrogen-induced material damage is approximated by a parametric dependency of local fracture resistance (critical energy release rate) on hydrogen concentration. In order to illustrate the capability of the simulation method, we have demonstrated a ductile-brittle transition in the failure pattern of a double edge notched specimen under tension w/ and w/o hydrogen charging.

The presented modelling and simulation approach for the fracture mechanics-based assessment of hydrogen-sensitive applications could enable a controlled use of high strength alloys, accelerate material certification, and govern inspection planning and fitness-for-service assessment.

References

[1] W. Johnson, "On some remarkable changes produced in iron and steel by the action of hydrogen and acids," *Proce. Roy. Soc. London,* vol. 23, p. 168–179, 1875. https://doi.org/10.1098/rspl.1874.0024.

[2] R. P. Gangloff, "Hydrogen-assisted Cracking," in *Comprehensive Structural Integrity*, vol. 6, R. Ritchie, B. Karihaloo and I. Milne, Eds., New York, 2003. https://doi.org/10.1016/B0-08-043749-4/06134-6, pp. 31-101.

[3] R. Fernandez-Sousa, C. Betegon and E. Martínez-Paneda, "Analysis of the influence of microstructural traps on hydrogen assisted fatigue," *Acta Mater.,* vol. 199, pp. 253-263, 2020. https://doi.org/10.1016/j.actamat.2020.08.030.

[4] R. Gangloff and B. Somerday, Gaseous Hydrogen Embrittlement of Materials in Energy Technologies, Cambridge: Woodhead Publishing Limited, 2012.

[5] M. Djukic, G. Bakic, V. Sijacki Zeravcic, A. Sedmak and B. Rajicic, "The synergistic action and interplay of hydrogen embrittlement mechanisms in steels and iron: Localized plasticity and decohesion," *Eng. Fract. Mech.,* no. 216, p. 106528, 2019. https://doi.org/10.1016/j.engfracmech.2019.106528.

[6] H. K. Birnbaum and P. Sofronis, "Hydrogen-enhanced localized plasticity - a mechanism for hydrogen related fracture," *Mater. Sci. Eng.,* no. A 176, pp. 191-202, 1994. https://doi.org/10.1016/0921-5093(94)90975-X.

[7] Z. D. Harris, S. K. Lawrence, D. L. Medlin, G. Guetard, J. T. Burns and B. P. Somerday, "Elucidating the contribution of mobile hydrogen-deformation interactions to hydrogen-induced intergranular cracking in polycristalline nickel," *Acta Mater.,* no. 218, pp. 180-192, 2018. https://doi.org/10.1016/j.actamat.2018.07.043.

[8] E. Martínez-Paneda, V. S. Deshpande, C. F. Niordson and N. A. Fleck, "The role of plastic strain gradients in crack growth resistance of metals," *J. Mech. Phys. Solids,* no. 126, pp. 136-150, 2019. https://doi.org/10.1016/j.jmps.2019.02.011.

[9] S. S. Shishvan, G. Csanyi and V. S. Deshpande, "Hydrogen induced fast-fracture," *J. Mech. Phys. Solids,* no. 134, p. 103740, 2020. https://doi.org/10.1016/j.jmps.2019.103740.

[10] A. Diaz, J. M. Alegre, I. I. Cuesta and Z. Zhang, "Explicit implementation of hydrogen transport in metals," *International Journal of Mechanical Sciences,* vol. 273, p. 109195, 2024. https://doi.org/10.1016/j.ijmecsci.2024.109195.

[11] A. D. V. Raina, E. Martinez-Paneda and N. Fleck, "Analysis of hydrogen diffusion in the three stage electro-permeation test," *Continuum Mechanics and Thermodynamics,* vol. 36, p. 1169–1180, 2024. https://doi.org/10.1007/s00161-023-01237-5.

[12] R. A. Oriani, "The diffusion and trapping of hydrogen in steel," *Acta Metall,* vol. 18, pp. 147-157, 1970. https://doi.org/10.1016/0001-6160(70)90078-7.

[13] H. Yu, A. Diaz, X. Lu, B. Sung, Y. Ding, M. Koyama, J. He, X. Zhu, A. Oudriss, X. Feaugass and Z. Zhang, "Hydrogen Embrittlement as a Conspicuous Material Challenge - Comprehensive Review and Future Directions," *Chem. Rev.,* no. 124, pp. 6271-6392, 2024. https://doi.org/10.1021/acs.chemrev.3c00624.

[14] P. Kristensen, C. Niordson and E. Martinez-Paneda, "Applications of phase field fracture in modelling hydrogen assisted failures," *Theoretical and Applied Fracture Mechanics,* vol. 110, p. 102837, 2020. https://doi.org/10.1016/j.tafmec.2020.102837.

[15] H. Bhadeshia, „Prevention of Hydrogen Embrittlement in Steels,“ *ISIJ International, Vol. 56 (2016), N,* Bd. 56, Nr. 1, pp. 24-36, 2016. https://doi.org/10.2355/isijinternational.ISIJINT-2015-430.

[16] K. Pham, H. Amor, J.-J. Marigo and C. Maurini, "Gradient damage models and their use to approximate brittle fracture," *Int. J. Damage Mech.*, vol. 20, pp. 618-652, 2011. https://doi.org/10.1177/1056789510386852.

[17] E. Tanne, T. Li, B. Bourdin, J.-J. Marigo and C. Maurini, "Crack nucleation in variational phase-field models of brittle fracture," *Journal of the Mechanics and Physics of Solids*, vol. 110, pp. 80-99, 2018. https://doi.org/10.1016/j.jmps.2017.09.006.

[18] L.-C. Hwang and T.-P. Perng, "Hydrogen transport in ferritic stainless steel under elastic stress," *Materials Chemistry and Physics,*, no. 36, pp. 231-235, 1994. https://doi.org/10.1016/0254-0584(94)90034-5.

[19] H. Hagi, "Diffusion Coefficient of Hydrogen in Iron without Trapping by Dislocations and Impurities," *Materials Transactions, JIM,* vol. 35, no. 2, pp. 112-117, 1994. https://doi.org/10.2320/MATERTRANS1989.35.112.

[20] H. Katsuta and K. Furkawa, "Hydrogen and Deuterium Transport through Type 304 Stainless Steel at Elevated Temperatures," *Journal of Nuclear Science and Technology*, vol. 18, no. 2, pp. 143-151, 1981. https://doi.org/10.1080/18811248.1981.9733235.

Stefan Lampenscherf
Cheruskerweg 8, 85586 Poing, Germany
lightsharp30@outlook.de

Gia Khanh Pham
Munich University of Applied Sciences
Lothstr. 34, 80335 München, Germany
gia-khanh.pham@hm.edu